MNRAS **000**, 000–000 (0000) Preprint 8 March 2024 Compiled using MNRAS LATEX style file v3.0

The diverse density profiles of galaxy clusters with self-interacting dark matter plus baryons

Andrew Robertson⋆,[1] Richard Massey,[1] Vincent Eke,[1] Sean Tulin,[2] Hai-Bo Yu,[3] Yannick Bahé,[4,5] David J. Barnes,[6,7] Richard G. Bower,[1] Robert A. Crain,[8] Claudio Dalla Vecchia,[9,10] Scott T. Kay,[6] Matthieu Schaller[1,4] and Joop Schaye[4]

[1] *Institute for Computational Cosmology, Durham University, South Road, Durham DH1 3LE, UK*
[2] *Department of Physics and Astronomy, York University, Toronto, Ontario M3J 1P3, Canada*
[3] *Department of Physics and Astronomy, University of California, Riverside, California 92521, USA*
[4] *Leiden Observatory, Leiden University, PO Box 9513, NL-2300 RA Leiden, the Netherlands*
[5] *Max-Planck-Institut für Astrophysik, Karl-Schwarzschild Str. 1, 85748 Garching, Germany*
[6] *Jodrell Bank Centre for Astrophysics, School of Physics and Astronomy, The University of Manchester, Manchester M13 9PL, UK*
[7] *Department of Physics, Kavli Institute for Astrophysics and Space Research, Massachusetts Institute of Technology, Cambridge, MA 02139, USA*
[8] *Astrophysics Research Institute, Liverpool John Moores University, 146 Brownlow Hill, Liverpool L3 5RF, United Kingdom*
[9] *Instituto de Astrofísica de Canarias, C/ Vía Láctea s/n, 38205 La Laguna, Tenerife, Spain*
[10] *Departamento de Astrofísica, Universidad de La Laguna, Av. del Astrofísico Francisco Sánchez s/n, 38206 La Laguna, Tenerife, Spain*

arXiv:1711.09096v2 [astro-ph.CO] 22 Feb 2018

8 March 2024

ABSTRACT

We present the first simulated galaxy clusters ($M_{200} > 10^{14}\,\mathrm{M}_\odot$) with both self-interacting dark matter (SIDM) and baryonic physics. They exhibit a greater diversity in both dark matter and stellar density profiles than their counterparts in simulations with collisionless dark matter (CDM), which is generated by the complex interplay between dark matter self-interactions and baryonic physics. Despite variations in formation history, we demonstrate that analytical Jeans modelling predicts the SIDM density profiles remarkably well, and the diverse properties of the haloes can be understood in terms of their different final baryon distributions.

Key words: dark matter — astroparticle physics — cosmology: theory — galaxies: clusters: general

1 INTRODUCTION

The possibility that dark matter (DM) particles can interact with one another through forces other than just gravity has received significant attention since it was first proposed by Spergel & Steinhardt (2000). The existence of self-interacting dark matter (SIDM) would have significant implications for both particle physics and astrophysics. A detection of significant self-interactions would rule out many popular DM candidates such as axions (Duffy & van Bibber 2009) or supersymmetric neutralinos (Bertone et al. 2005), and would alter cosmological structure formation on small scales. SIDM would explain why many dwarf and low surface brightness galaxies appear to have less DM in their centres than is predicted when DM particles are assumed to be collisionless (Rocha et al. 2013; Vogelsberger et al. 2014; Elbert et al. 2015). It also provides a mechanism to produce a *diversity* of DM density profiles (Elbert et al. 2016; Creasey et al. 2017; Kamada et al. 2017) that is difficult to achieve within the standard paradigm (Oman et al. 2015), and appears to be necessary if DM density profiles are being correctly inferred from observations (e.g. de Blok et al. 2008; Kuzio de Naray et al. 2008; Adams et al. 2014; Oh et al. 2015).

The mechanism by which SIDM alters the density profile of a halo is thermalization. Self-interactions redistribute energy between particles, heating up the centre of the halo, which would otherwise have a low velocity dispersion. These heated particles move to orbits with larger apocenters, shifting mass from the centre to larger radii. Regions where SIDM particles have scattered multiple times approach thermal equilibrium, which has led to the modelling of SIDM as an isothermal gas (Kaplinghat et al. 2014), known as *Jeans modelling*. A key prediction of this method is that baryons play an important role in determining the final SIDM profile, with slight differences in baryonic distributions leading to very different rotation curves (Kamada et al. 2017).

The high densities and velocity dispersions in galaxy clusters mean that for a given SIDM cross-section, the ther-

⋆ e-mail: andrew.robertson@durham.ac.uk

© 0000 The Authors

malisation timescales are shorter than in individual galaxies. These systems can therefore provide strong constraints on the self-interaction properties of DM. At the same time, physical processes within a cluster span a large dynamical range, making them computationally expensive to study using N-body simulations. Analytical methods can be applied to these massive systems, but it is important to verify that these methods work.

This letter introduces the first simulations of galaxy clusters to incorporate both SIDM and the baryonic processes that are important for galaxy formation. These simulated clusters provide an ideal way to test constraints placed on the SIDM cross-section from observed clusters, and are used here to explicitly test Jeans modelling of SIDM. We introduce the simulations in §2, before discussing the density profiles of our simulated clusters in §3. We conclude in §4.

2 SIMULATIONS

2.1 The Cluster-EAGLE simulations

We have re-simulated two clusters from the Cluster-EAGLE (C-EAGLE) project (Bahé et al. 2017; Barnes et al. 2017b): CE-05 and CE-12, with masses of $M_{200} = 1.4$ and $3.9 \times 10^{14}\,\mathrm{M}_\odot$ respectively.[1] Both clusters are classified as 'relaxed', based on their gas properties at $z = 0.1$ (Barnes et al. 2017b). We ran four simulations of each cluster: CDM-only, CDM+baryonic physics, SIDM-only and SIDM+baryonic physics. An isotropic and velocity-independent cross-section of $\sigma/m = 1\,\mathrm{cm}^2\,\mathrm{g}^{-1}$ was used for all runs with SIDM.

The C-EAGLE project uses the zoom simulation technique (Katz & White 1993) to resimulate (at higher resolution) galaxy cluster haloes found in a parent simulation with a side length of 3.2 Gpc (Barnes et al. 2017a). The high-resolution region around each cluster is selected so that no lower resolution particles are present within a radius of $5\,r_{200}$ from the cluster centre at $z = 0$. The high-resolution region matches the resolution of the EAGLE 100 Mpc simulation (Ref-L100N1504, Schaye et al. 2015), with DM particle mass $m_{\mathrm{DM}} = 9.7 \times 10^6\,\mathrm{M}_\odot$ and initial gas particle mass $m_{\mathrm{gas}} = 1.8 \times 10^6\,\mathrm{M}_\odot$. Runs including baryons used the EAGLE galaxy formation model (Schaye et al. 2015; Crain et al. 2015), which includes radiative cooling, star formation, stellar evolution, feedback due to stellar winds and supernovae, and the seeding, growth and feedback from black holes. The specific calibration of EAGLE that was used, is labelled as '*AGNdT9*' in Schaye et al. (2015). This was chosen as it provides a better match to the observed gas fraction and X-ray luminosity–temperature relation of galaxy groups than the fiducial '*Ref*' calibration. All the simulations used a *Planck* 2013 cosmology (Planck Collaboration et al. 2014).[2]

Because this work focusses on radial density profiles, we here summarise the strengths and weaknesses of C-EAGLE in this respect. C-EAGLE clusters simulated in a CDM universe have total stellar content and black hole masses that match observed relations (Bahé et al. 2017), but their central galaxies are ≈ 3 times too massive. The simulated clusters are slightly too gas rich overall, but have a deficit of gas in their centres, where the gas is also too hot (Barnes et al. 2017b). Star particles in EAGLE lose mass to the surrounding gas, which can lead to the formation of massive gas particles in gas-poor regions. We have found that both the CDM and SIDM versions of CE-05 form a single massive gas particle at the centre of the halo. The density profile of this particle, using its SPH kernel, is shown as a dashed line in Figure 1.

2.2 Implementation of dark matter scattering

During each simulation time-step, DM particles search for neighbours within a radius h_{SI}, and scatter isotropically with probability

$$P_{\mathrm{scat}} = \frac{(\sigma/m)\; m_{\mathrm{DM}}\, v\, \Delta t}{\frac{4\pi}{3} h_{\mathrm{SI}}^3}, \tag{1}$$

where v is the particles' relative velocity, and Δt is the size of the time-step (Robertson et al. 2017). Provided it is smaller than resolved structures, the results are insensitive to the exact choice of h_{SI} (Robertson 2017). We therefore fix h_{SI} to a constant comoving size of 2.66 kpc, matching the gravitational softening length in EAGLE before $z = 2.8$.

2.3 Structural properties of simulated clusters

The properties of the clusters at z=0 are listed in Table 1. As well as the total, stellar and gas mass within r_{200}, we show the parameters of a fit to the density profiles of our DM-only runs. For CDM, we fit a Navarro et al. (1997, NFW) profile

$$\frac{\rho_{\mathrm{NFW}}(r)}{\rho_{\mathrm{crit}}} = \frac{\delta_{\mathrm{NFW}}}{(r/r_{\mathrm{s}})(1 + r/r_{\mathrm{s}})^2}, \tag{2}$$

where r_{s} is a scale radius, δ_{NFW} a dimensionless characteristic density, and $\rho_{\mathrm{crit}} = 3H^2/8\pi G$ is the critical density. The NFW concentration parameter is defined as $c_{200} \equiv r_{200}/r_{\mathrm{s}}$. For SIDM runs, we fit a Burkert (1995) profile

$$\rho_{\mathrm{B}}(r) = \frac{\rho_{\mathrm{b}}\, r_{\mathrm{b}}^3}{(r + r_{\mathrm{b}})(r^2 + r_{\mathrm{b}}^2)}, \tag{3}$$

which has a constant density core inside radius r_{b}. All fits were performed between radii $0.01\,r_{200}$ and r_{200}, minimising

$$\sum_{i=1}^{N_{\mathrm{bins}}} \left(\log \rho_{\mathrm{sim}}(r_i) - \log \rho_{\mathrm{fit}}(r_i)\right)^2, \tag{4}$$

where the $N_{\mathrm{bins}} = 50$ radial bins are logarithmically spaced. The CDM-only profiles are well fit at radii outside 10 kpc, but exceeded the NFW model in the very centre. Both SIDM-only profiles are well fit on all scales (see also Rocha et al. 2013).

For each simulated halo, we also calculate the Bullock et al. (2001) dimensionless spin parameter

$$\lambda' \equiv \frac{|\boldsymbol{J}|}{\sqrt{2} M_{200} V_{200} r_{200}}, \tag{5}$$

where $\boldsymbol{J}$ is the angular momentum of all mass within r_{200}, about the most-bound particle. The velocities in $\boldsymbol{J}$ are with respect to the mass-weighted average velocity of the halo.

[1] We define r_{200} as the radius at which the mean enclosed density is 200 times the critical density, and M_{200} as the mass within r_{200}.
[2] Specifically, $\Omega_{\mathrm{b}} = 0.04825$, $\Omega_{\mathrm{m}} = 0.307$, $\Omega_\Lambda = 0.693$, $H_0 = 67.77\,\mathrm{km\,s^{-1}\,Mpc^{-1}}$, $\sigma_8 = 0.8288$, $n_{\mathrm{s}} = 0.9611$ and $Y = 0.248$.

Halo	Physics	M_{200} [$10^{14}\,M_\odot$]	r_{200} [Mpc]	M_* [$10^{12}\,M_\odot$]	$M_{\rm gas}$ [$10^{12}\,M_\odot$]	$f_{\rm bar}$ [%]	c_{200}	$r_{\rm b}$ [kpc]	λ'	$M_*(<30\,{\rm kpc})$ [$10^{12}\,M_\odot$]	$M_{\rm DM}(<30\,{\rm kpc})$ [$10^{12}\,M_\odot$]	$t^*_{1/2}$ [Gyr]
CE-05	CDM	1.37	1.09				6.40		0.027			
	CDM+baryon	1.38	1.09	1.86	13.7	10.5			0.027	0.49	1.48	3.8
	SIDM	1.36	1.08					95	0.028			
	SIDM+baryon	1.36	1.09	1.95	12.9	10.9			0.029	0.61	1.02	4.3
CE-12	CDM	3.92	1.54				4.35		0.036			
	CDM+baryon	3.96	1.55	5.74	53.8	15.0			0.040	0.58	1.21	6.8
	SIDM	3.88	1.54					199	0.036			
	SIDM+baryon	3.91	1.54	5.85	52.2	14.9			0.039	0.24	0.26	5.3

Table 1. The $z = 0$ properties of the two halos, in each of the four Physics runs. M_* and $M_{\rm gas}$ are the total stellar and gas masses within r_{200}, while $f_{\rm bar}$ is the baryon fraction within r_{200}. The concentration, c_{200}, of each halo was only calculated for the CDM-only simulations. Similarly, the Burkert scale radius, $r_{\rm b}$, was only calculated for SIDM-only simulations. λ' is the halo spin parameter, including all mass within r_{200}. $M_*(<30\,{\rm kpc})$ and $M_{\rm DM}(<30\,{\rm kpc})$ are measurements of the stellar and DM mass within a 30 kpc spherical aperture, centred on the most bound particle. $t^*_{1/2}$ is the age of the universe when $M_*(<30\,{\rm kpc})$ was 50% of its $z = 0$ value.

3 HALO DENSITY PROFILES

3.1 Simulation results

When baryons are added to CDM simulations (top panels of Figure 1), stars dominate the central 10 kpc of the total mass profile, but the DM density profile stays almost unchanged. When baryons are added to SIDM haloes (bottom panels), the response of the two clusters is starkly different. The SIDM halo of CE-12 develops a large core of constant DM density, with or without baryons. The density of stars in its inner 20 kpc is less than half of that with CDM+baryons, but with a similar radial dependence. On the other hand, including baryons in CE-05 enhances the central DM density relative to the SIDM-only run, removing the constant density core and recovering a cuspy total density profile that differs only slightly from that with CDM+baryons.

3.2 Semi-analytic Jeans modelling of SIDM

The contrast between the cored SIDM profile of CE-12, which is unaffected by baryons, versus the creation of an SIDM cusp in the baryonic version of CE-05, is a consequence of the two clusters' different baryonic distributions. Kaplinghat et al. (2016) successfully fit the rotation curves of simulated SIDM halos using a model where SIDM behaves as an isothermal gas within the radius (known as r_1) at which particles have scattered once over the age of the halo. The density profile in this isothermal regime is predicted by solving Poisson's equation, while requiring hydrostatic equilibrium.[3] The results of this procedure (using M_{200} and c from the CDM-only simulations, the baryon distribution from SIDM+baryons, and the true cross-section of $\sigma/m = 1\,{\rm cm^2\,g^{-1}}$ as inputs) are shown in Figure 1, and are an excellent match to the SIDM density measured in both SIDM+baryons simulations.

In the inner regions of our haloes, where the baryons dominate, this analytical prescription leads to a DM density profile (Kaplinghat et al. 2014)

$$\rho_{\rm DM}(r) \approx \rho_0 \exp\left\{\frac{\Phi_{\rm B}(0) - \Phi_{\rm B}(r)}{\sigma_0^2}\right\}, \quad (6)$$

where ρ_0 is the central DM density, $\Phi_{\rm B}$ is the gravitational potential due to the baryonic mass distribution, and σ_0 is the one-dimensional velocity dispersion of SIDM (which is approximately constant inside r_1, because DM interactions efficiently redistribute energy between SIDM particles).

From equation (6) we can see that the density in the inner regions of the DM halo will be roughly constant if $|\Phi_{\rm B}(0)| < \sigma_0^2$, while it will increase towards smaller radii if the baryonic potential is significant compared with the DM velocity dispersion. For halos that have been thermalised by DM self-interactions, the central velocity dispersion is roughly the maximum (across all radii) velocity dispersion that the halo would have in the absence of self-interactions (see Figure 6 of Rocha et al. 2013). This in turn is about $0.66\,v_{\rm max}$, independent of the halo mass or concentration (Łokas & Mamon 2001), where $v_{\rm max} \equiv \max\left\{\sqrt{GM(<r)/r}\right\}$ is the maximum circular velocity of the halo.

For CE-05, $v_{\rm max} = 848\,{\rm km\,s^{-1}}$ and $\sqrt{|\Phi_{\rm B}(0)|} = 1050\,{\rm km\,s^{-1}}$, while for CE-12, $v_{\rm max} = 1107\,{\rm km\,s^{-1}}$ and $\sqrt{|\Phi_{\rm B}(0)|} = 800\,{\rm km\,s^{-1}}$.[4] The different behaviour of SIDM in CE-05 and CE-12 is therefore readily understood as a result of the much deeper baryonic potential well in CE-05, combined with CE-12 being more massive (and so with higher DM velocity dispersion). Importantly, Jeans modelling produces an excellent match to the DM density in *both* SIDM+baryons simulations, adding credence to cross-sections inferred from observational data using this method (Kaplinghat et al. 2016; Kamada et al. 2017).

3.3 Discussion

While the SIDM density profiles can be explained in light of the associated baryonic potentials, it is not clear what gave rise to these two haloes having quite different central stellar distributions. After all, the density profiles of the stars in the CDM+baryons versions of CE-05 and CE-12 are similar

[3] The temperature of this 'isothermal gas', is related to the SIDM velocity dispersion, such that the SIDM follows the ideal gas law $p = \rho\,\sigma_0^2$, where p and ρ are the SIDM pressure and density and σ_0 is the one-dimensional velocity dispersion.

[4] $\Phi_{\rm B}(r)$ was calculated from the radial density profiles of stars and gas, assuming spherical symmetry.

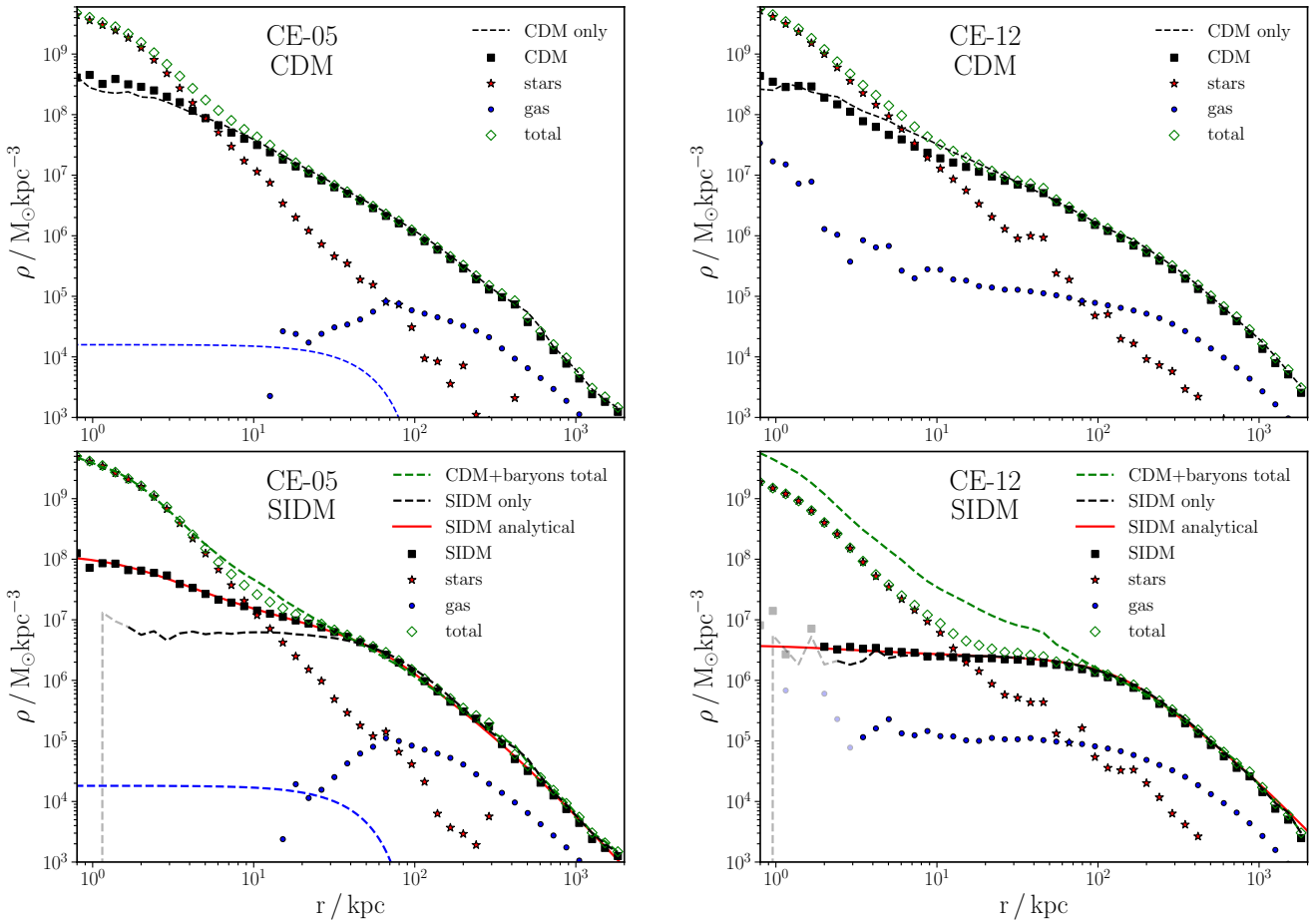


Figure 1. The $z = 0$ radial density profiles of CE-05 (left) and CE-12 (right), with CDM (top) and SIDM (bottom). The DM-only density profiles are overlaid as black dashed lines, and the SIDM panels have the total density profiles from their CDM counterparts overlaid as green dashed lines. Symbols and lines become semi-transparent when the density corresponds to fewer than 10 particles per radial bin. The solid red lines in the bottom panels are the analytical predictions for the SIDM density, discussed in Section 3.2. The blue dashed lines are the density profiles of single massive gas particles that form at the centre of CE-05 (see Section 2.1).

to one another and to that in the SIDM+baryons version of CE-05. The interesting question is then why SIDM has a large effect on the stellar distribution only in CE-12.

As can be seen in Table 1, neither halo has particularly unusual structural parameters. The concentrations of the CDM-only CE-05 and CE-12 are 6.4 and 4.4 respectively. Given their masses, this places them $0.7\,\sigma$ above and $0.4\,\sigma$ below the Correa et al. (2015) concentration-mass relation, assuming concentrations to be log-normally distributed with $\sigma_{\log_{10} c} = 0.1$ (Dolag et al. 2004). The halo spins are also unremarkable: the $\lambda' = 0.027$ and 0.036 values from our CDM-only simulations are within the typical scatter seen in larger simulations, which have median $\lambda' \approx 0.035$ independent of halo mass, and $\sigma_{\log_{10} \lambda'} \approx 0.22$ (e.g. Bullock et al. 2001; Macciò et al. 2007).

Any differences between the $z = 0$ properties of haloes with SIDM+baryons must ultimately be traceable back to the initial conditions, and should therefore show up in the CDM-only runs. However, even with CDM, the concentration, spin, sphericity, triaxiality, substructure and environment of a halo cannot fully explain the scatter in stellar masses at fixed halo mass (Matthee et al. 2017). One notable difference between the haloes is that CE-05 undergoes a 6:1 mass merger at $z \approx 0.2$. However, the qualitative features of CE-05's density profile are the same at $z = 0.3$ (before the merger has taken place) as at $z = 0$. This merger therefore does not affect our conclusions.

Turning to the CDM+baryons runs, there are significant differences in the timescale for the build-up of stellar mass within the central galaxy (the BCG). At $z = 0$, the clusters have a similar stellar mass within a 30 kpc spherical aperture. For CE-05, half of that stellar mass was already inside this aperture 3.8 Gyr after the Big Bang. The same milestone was reached 3 Gyr later in CE-12. SIDM interactions take time to influence the structure of a halo, and are unable to significantly do so in the presence of a deep baryonic potential well. A BCG that builds up its stellar mass early, may therefore resist the effect of DM interactions to reduce the central DM density. Coupled to the fact that CE-12 is a more massive cluster, with a correspondingly larger SIDM temperature, and so more resilience to the inclusion of baryons, the different early formation histories of these haloes may explain why they react so differently to the inclusion of DM interactions by $z = 0$.

Importantly, the SIDM+baryons version of CE-12 does not contain fewer stars than the CDM+baryons version –

just fewer stars in the central galaxy. This could be a result of the reduced dynamical friction in a cored density profile (Read et al. 2006; Petts et al. 2015), leading to less accretion of stellar mass from satellite galaxies.

4 CONCLUSIONS

We have produced the first simulations of galaxy clusters to include both SIDM and baryonic physics. Of our two simulated SIDM+baryon clusters, one has a large constant density DM core, while the other has a cuspy DM density profile more reminiscent of CDM. We demonstrated that the analytical model introduced in Kaplinghat et al. (2014) can successfully explain the behaviour of our two haloes: the cuspy SIDM halo has a deep baryonic potential, while the cored halo belongs to a system with a much shallower baryonic potential. What is responsible for these clusters having different central distributions of baryons (mainly stars) is hard to infer from only two simulated systems, but we speculate that the early formation time of the central galaxy in one of our clusters may explain why it is relatively unaffected by DM self-interactions.

Ultimately, the different response between the two haloes to the inclusion of SIDM may not be simply related to the parameters of the CDM haloes, or to their formation history. The complex interplay at the centre of a cluster between gas cooling, gravitational collapse and AGN feedback is highly non-linear, and the behaviour of SIDM in the presence of a dense or diffuse baryonic component provides a positive feedback mechanism. Less dense systems are made even less dense by DM self-interactions, while dense systems are relatively unaffected by these interactions. The large differences between our two systems suggest that mapping the full diversity of cluster haloes with SIDM will require simulations of more systems (including baryons).

Encouragingly, analytical Jeans modelling of SIDM reproduces the density profiles in the simulations. Even though the distribution of baryons and SIDM are hard to predict from the CDM properties of a halo, knowledge of the baryon distribution allows one to predict the SIDM distribution for a given cross-section. This is relevant for the interpretation of observed systems, where the baryon distribution can be observed, and (for different SIDM cross-sections) the predicted DM distributions can be compared with kinematic and gravitational lensing data to infer the best fitting self-interaction cross-section.

ACKNOWLEDGMENTS

This work was made possible by Lydia Heck's technical support and expertise. Thanks also to Subir Sarkar, Felix Kahlhoefer, Kai Schmidt-Hoberg and Torsten Bringmann for organising an excellent SIDM workshop in Copenhagen, and Manoj Kaplinghat, David Harvey and Mathilde Jauzac for helpful discussions.

This work was supported by the UK Science and Technology Facilities Council, through grants ST/K501979/1, ST/L00075X/1 and ST/L000768/1. It used the DiRAC Data Centric system at Durham University, operated by the Institute for Computational Cosmology on behalf of the STFC DiRAC HPC Facility (www.dirac.ac.uk). This equipment was funded by BIS National E-infrastructure capital grant ST/K00042X/1, STFC capital grants ST/H008519/1 and ST/K00087X/1, STFC DiRAC Operations grant ST/K003267/1 and Durham University. This project also received funding from the EU Horizon 2020 research and innovation programme under Marie Skłodowska-Curie grant agreement 747645. The C-EAGLE simulations were in part performed on the German federal maximum performance computer "Hazel Hen" at the maximum performance computing centre Stuttgart (HLRS), under project GCS-HYDA / ID 44067 financed through the large-scale project "Hydrangea" of the Gauss Centre for Supercomputing. Further simulations were performed at the Max Planck Computing and Data Facility in Garching, Germany. RM and RC were supported by the Royal Society, and HBY by the US Department of Energy (grant de-sc0008541) and the Hellman Fellows Fund. CDV acknowledges financial support from the Spanish Ministry of Economy and Competitiveness (MINECO) through grants AYA2014-58308 and RYC-2015-1807.

REFERENCES

Adams J. J., et al., 2014, ApJ, 789, 63
Bahé Y. M., et al., 2017, MNRAS, 470, 4186
Barnes D. J., Kay S. T., Henson M. A., McCarthy I. G., Schaye J., Jenkins A., 2017a, MNRAS, 465, 213
Barnes D. J., et al., 2017b, MNRAS, 471, 1088
Bertone G., Hooper D., Silk J., 2005, Phys. Rep. , 405, 279
Bullock J. S., Dekel A., Kolatt T. S., Kravtsov A. V., Klypin A. A., Porciani C., Primack J. R., 2001, ApJ, 555, 240
Burkert A., 1995, ApJ , 447, L25
Correa C. A., Wyithe J. S. B., Schaye J., Duffy A. R., 2015, MNRAS, 452, 1217
Crain R. A., et al., 2015, MNRAS, 450, 1937
Creasey P., Sameie O., Sales L. V., Yu H.-B., Vogelsberger M., Zavala J., 2017, MNRAS, 468, 2283
Dolag K., Bartelmann M., Perrotta F., Baccigalupi C., Moscardini L., Meneghetti M., Tormen G., 2004, A&A , 416, 853
Duffy L. D., van Bibber K., 2009, New J. Phys. , 11, 105008
Elbert O. D., Bullock J. S., Garrison-Kimmel S., Rocha M., Oñorbe J., Peter A. H. G., 2015, MNRAS, 453, 29
Elbert O. D., Bullock J. S., Kaplinghat M., Garrison-Kimmel S., Graus A. S., Rocha M., 2016, preprint, (arXiv:1609.08626)
Kamada A., Kaplinghat M., Pace A. B., Yu H.-B., 2017, PRL , 119, 111102
Kaplinghat M., Keeley R. E., Linden T., Yu H.-B., 2014, PRL , 113, 021302
Kaplinghat M., Tulin S., Yu H.-B., 2016, PRL , 116, 041302
Katz N., White S. D. M., 1993, ApJ, 412, 455
Kuzio de Naray R., McGaugh S. S., de Blok W. J. G., 2008, ApJ, 676, 920
Łokas E. L., Mamon G. A., 2001, MNRAS, 321, 155
Macciò A. V., Dutton A. A., van den Bosch F. C., Moore B., Potter D., Stadel J., 2007, MNRAS, 378, 55
Matthee J., Schaye J., Crain R. A., Schaller M., Bower R., Theuns T., 2017, MNRAS, 465, 2381
Navarro J. F., Frenk C. S., White S. D. M., 1997, ApJ, 490, 493
Oh S.-H., et al., 2015, AJ , 149, 180
Oman K. A., et al., 2015, MNRAS, 452, 3650
Petts J. A., Gualandris A., Read J. I., 2015, MNRAS, 454, 3778
Planck Collaboration et al., 2014, A&A , 571, A16
Read J. I., Goerdt T., Moore B., Pontzen A. P., Stadel J., Lake G., 2006, MNRAS, 373, 1451

Robertson A., 2017, PhD thesis, Durham University, http://etheses.dur.ac.uk/12305/
Robertson A., Massey R., Eke V., 2017, MNRAS, 465, 569
Rocha M., Peter A. H. G., Bullock J. S., Kaplinghat M., Garrison-Kimmel S., Oñorbe J., Moustakas L. A., 2013, MNRAS, 430, 81
Schaye J., et al., 2015, MNRAS, 446, 521
Spergel D. N., Steinhardt P. J., 2000, PRL , 84, 3760
Vogelsberger M., Zavala J., Simpson C., Jenkins A., 2014, MNRAS, 444, 3684
de Blok W. J. G., Walter F., Brinks E., Trachternach C., Oh S.-H., Kennicutt Jr. R. C., 2008, AJ , 136, 2648

This paper has been typeset from a TEX/LATEX file prepared by the author.